Facile Fabrication of Hierarchical Porous N/O Functionalized Carbon Derived from Blighted Grains Towards Electrochemical Capacitors

Chen Zhiyi[1,2], *Wang Zhengluo*[1,2], *Zhao Zhiwei*[2], *Sun Xuan*[1], *Hou Linrui*[1,2*], *Yuan Changzhou*[1,2*]

1. School of Materials Science and Engineering, University of Jinan, Jinan 250022, P. R. China;
2. School of Materials Science and Engineering, Anhui University of Technology, Ma'anshan 243002, P. R. China

(Received 10 May 2018, revised 30 June 2018, accepted 11 July 2018)

Abstract: The hierarchical porous N/O co-functionalized carbon (HPNOC) was scalably prepared by using the low-cost and renewable blighted grains as the raw material coupled with mild $KHCO_3$ activation for electrochemical capacitors (ECs). The elemental N was in situ doped in the obtained HPNOC without any N-containing additives. Remarkably, the obtained HPNOC was endowed with a large specific surface area (about 2 624 $m^2 \cdot g^{-1}$), high pore volume (about 1.35 $cm^3 \cdot g^{-1}$), as well as high-content N/O functionalization (about 1.9% (in atom) N and about 10.2% (in atom) O. Furthermore, the as-resulted HPNOC electrode with a high mass loading of 5 $mg \cdot cm^{-2}$ exhibited competitive gravimetric capacitances of about 373.6 $F \cdot g^{-1}$ at 0.5 $A \cdot g^{-1}$, and even about 260.4 $F \cdot g^{-1}$ at a high rate of 10 $A \cdot g^{-1}$; superior capacitance retention of about 98.8% at 1 $A \cdot g^{-1}$ over 10 000 consecutive cycles; and high specific energy of about 9.6 $W \cdot h \cdot kg^{-1}$ at a power of 500 $W \cdot kg^{-1}$, when evaluated as a promising electrode in 6 mol KOH for advanced electrochemical supercapacitors. More encouragingly, the green synthetic strategy we developed holds a huge promise in generalizing for other biomass-derived carbon materials for versatile energy-related applications.

Key words: hierarchical porous carbon; $KHCO_3$ activation; N/O functionalization; electrochemical supercapacitors; eco-friendly fabrication

CLC number: TM912.9; TG456 **Document code**: A **Article ID**: 1005-1120(2018)04-0639-09

0 Introduction

Electrochemical supercapacitors, especially electric double-layer capacitors (EDLCs), have gained increasing attention for energy storage applications, particularly in high-power devices, owing to their fast charge/discharge capability and long-span cycling stability[1-3]. However, EDLCs still suffer seriously from low specific energy (SE), which greatly limits their practical applications. According to the classic formula ($SE=\frac{1}{2}CV^2$), SE can be improved by increasing the specific capacitance C and/or broadening the voltage window V of the cell. The intrinsic capacitance of EDLCs entirely originates from the pure charge accumulation at the electrode/electrolyte sur-/interfaces, thus large specific surface area (SSA) and suitable porous structure of the carbon electrodes are necessary for high-performance EDLCs electrodes[1,2]. In addition, the introduction of heteroatoms (N, P, S, etc.) is conducive to improve the ultimate capacitances of carbon materials. Elemental nitrogen and/or oxygen doping can further provide pseudocapacitance through the redox reactions[3,4], and meanwhile improve the electrode wettability[5,6]. Besides, the N species can enhance the conductivity of carbon materials themselves by adjusting the supply/acceptance of electrons in C atoms[3,4]. Nota-

* Corresponding author, E-mail address: mse_houlr@ujn.edu.cn, ayuancz@163.com.

How to cite this article: Chen Zhiyi, Wang Zhengluo, Zhao Zhiwei, et al. Facile fabrication of hierarchical porous N/O functionalized carbon derived from blighted grains towards electrochemical capacitors[J]. Trans. Nanjing Univ. Aero. Astro., 2018,35(4):639-647.
http://dx.doi.org/10.16356/j.1005-1120.2018.04.639

bly, the elemental oxygen is generally an ineluctably concomitant species in the porous carbon materials. As a contrast, the heteroatom of N should be purposefully introduced. What counts for practical applications of high-performance carbon electrodes is how to in situ dope the elemental N in the carbons without any extra N resource[7].

In common, biomass materials inherently with different heteroatoms are renewable/eco-friendly and abundant in nature, and can be further converted into advanced carbons with in situ doped heteroatoms. Until now, various biomasses, including popcorn[8], stiff silkworm[9], hexagonia apiaria[10], rose multiflora[11], cashmere[12], shiitake[13], lignite[14], and so on, have been investigated for preparing high-performance carbon materials. It is particularly worthy of noting that the highly corrosive and expensive KOH is always used as an activating agent for fabricating biomass-derived carbon-based materials[8-14], which is not beneficial for commercial applications. As a result, the exploration of low-cost and mild activating agents is still of great significance, and hugely challengeable.

Herein, we purposefully synthesized a hierarchical porous N/O functionalized carbon (HPNOC) from resourceful blighted grains by using the $KHCO_3$ as a mild and eco-friendly activator. Remarkably, the as-fabricated HPNOC electrode delivered high-rate capacitances and good cycling stability over 10 000 charge-discharge cycles in 6 mol KOH electrolyte, thanks to its unique porous architecture and striking N/O functionalization.

1 Experiment

1.1 Synthesis of HPNOC sample

Typically, the blighted grains were repetitiously washed with distilled water and absolute ethanol, and finally dried at 80 ℃ for 24 h. The dried blighted grains were pre-treated in a tubular furnace at 500 ℃ for 1 h, and the whole process was conducted under N_2 atmosphere. The obtained black powder was further mixed with the activation agent $KHCO_3$ with a mass ratio of 1∶3. Afterwards, the mixture was placed into a horizontal tube furnace and annealed under N_2 flow at 900 ℃ for 2 h, and then the sample was cooled to room temperature (RT). Subsequently, the resultant product was washed thoroughly with a 0.1 mol HCl solution and distilled water until the pH value reached 7. The final samples were gained after drying at 80 ℃. For comparison, the sample without the $KHCO_3$ activation was obtained via the same procedure as the HPNOC just with the absence of $KHCO_3$.

1.2 Characterizations

The structure and morphology of samples were confirmed by X-ray diffraction (XRD, Rigaku Ultima IV), scanning electron microscopy (SEM, JEOL-6300F), transmission electron microscopy (TEM) and high-resolution TEM (HRTEM, FEI TECNAI-20). The Raman analysis of the samples was recorded by LaserRaman (T6400, Jobion Yzon Corp.). X-ray photoelectron spectroscopy (XPS) was obtained via a VGESCALAB MKII X-ray photoelectron spectrometer. N_2 adsorption/desorption was determined by Brunauer-Emmett-Teller (BET) measurements using a TriStar II 3020ASAP-2020 surface area analyzer. BET equation was used to calculate the SSA of samples. The pore size distributions were evaluated by Barrett-Joyner-Halenda (BJH) and Density-Functional-Theory (DFT) methods.

1.3 Electrochemical measurements

The working electrodes were prepared with the electroactive material HPNOC, acetylene black and polytetrafluoroethylene (PTFE) in a weight ratio of 8∶1∶1. A small amount of deionized water was then added to obtain a more homogeneous mixture, which was pressed onto a Ni foam (1 cm × 1 cm) under a pressure of 15 MPa for following electrochemical measure-

ment in 6 Mol KOH solution. The typical loading of the active HPNOC on each electrode was 5 mg·cm^{-2}. Electrochemical characterization was performed in a three-electrode system, where a platinum plate (1 cm^2) and a saturated calomel electrode (SCE) were separately applied as the counter and reference electrodes at RT, or in two-electrode configuration with two identical electrodes face to face in 6 mol KOH electrolyte.

Electrochemical performances were conducted by cyclic voltammetry (CV), galvanostatic charge-discharge (GCD) measurements with an IVIUM electrochemical workstation (the Netherlands). The cycling stability was evaluated with a CT2001D tester (Wuhan, China). The specific capacitances (SCs) of the electrode or symmetric ECs were estimated from the CP curves based on the following equation

$$SC = \frac{It}{\Delta V}$$

where I, t and ΔV are the discharging current density (A·g^{-1}), discharging time (s) and discharging potential range (V) of the electrode or symmetric EC, respectively. Of note, I is calculated based on the two identical electrodes in the case of symmetric ECs. And the specific energy density (SED) and the specific power density (SPD) of the HPNOC-based symmetric ECs can be calculated using the following equations

$$SED = \frac{1}{2}SC(\Delta V)^2$$

$$SPD = SED/t$$

where SC is the capacitance of the symmetric device calculated based on the mass of the electroactive HPNOC in the two electrodes. The ΔV is for the working potential window of the HPNOC-based symmetric ECs.

2 Results and Discussion

2.1 Physicochemical characterization

Typical SEM image of the as-obtained HPNOC, as shown in Fig. 1(a), presents large interlaced sheets in micrometer size. Further TEM observations (Figs. 1(b), (c)) are conducted to examine the micro-structures of the HPNOC more clearly. Fig. 1(b) depicts the TEM image of the HPNOC. Obviously, a mass of highly interconnected pores and channels can be seen, in which electrolyte ions can diffuse and transport more easily. Furthermore, some structural defects and lattice disorder are evidently observed in the HRTEM image (Fig. 1(c)). Corresponding energy dispersive spectrometry elemental mapping analysis for the HPNOC specimen, as presented in Figs. 1(d)—(g), verifies the co-existence and uniform distributions of C, N and O species in the HPNOC product.

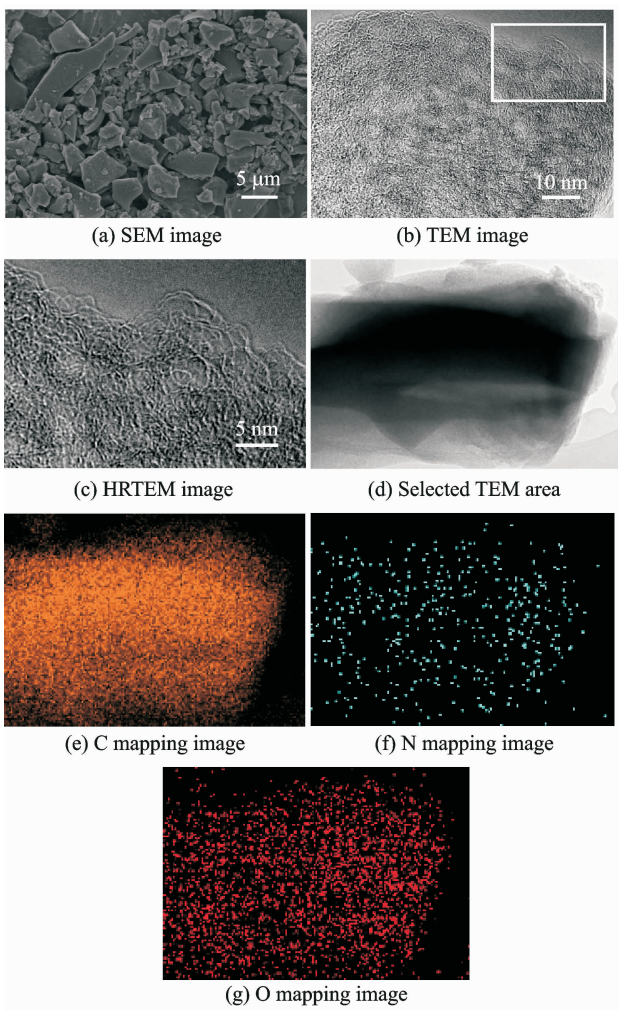

Fig. 1 SEM, TEM and HRTEM images for elements C, N and O of HPNOC sample

As observed in the XRD pattern of the HPNOC (Fig. 2(a)), two broad peaks of (002) and (100) at 2θ of about 22.8° and about 43.6° are related to disordered carbon and graphite (JCPDS

card No. 41-1487)[15], respectively. The high (002) peak intensity reveals the dominantly amorphous feature for the HPNOC, which accords well with the above HRTEM observation. As seen in the Raman spectrum (Fig. 2(b)), characteristic D and G bands centered at about 1 356.3 and 1 597.1 cm^{-1} are assigned to the non-perfect carbon structure and the sp^2-hybridized carbon framework[16], respectively. The I_G/I_D value is well fitted as about 0.43 for the HPNOC, which should result from the high-temperature $KHCO_3$ activation.

Figs. 2(c),(d) collected the high-resolution element XPS spectra of the HPNOC, and fitted profiles for the N and O species by the Gaussian fitting method. Specific information about the two elements is summarized in Table 1. As noted, corresponding chemical compositions of the HPNOC are estimated as about 87.9% (in atom) of carbon, about 1.9% (in atom) of nitrogen and about 10.2% (in atom) of oxygen according to the XPS measurement. Obviously, the N 1s spectrum (Fig. 2(c)) can be fitted into four typical peaks, representing pyridinic N (N-6, 26.2%, about 398.5 eV), pyrrolic N (N-5, 27.3%, about 399.8 eV), graphitic N (N-Q, 22.8%, about 401.5 eV) and oxidized N (N-X, 23.7%, about 402.5 eV)[17]. The high-content existence of the N-Q (about 0.43% (in atom)) and N-X (about 0.52% (in atom)) can hugely enhance the rapid electronic transfer through the carbon electrode[4, 11]. As for the O 1s (Fig. 2(d)), three configurations are determined, including the ethers and phenols type groups (O_1, 60.9%, about 533.1 eV), carbonyl groups (O_2, 33.4%, about 533.8 eV), and chemisorbed oxygen and/or water bonded to the carbon surface (O_3, 5.7%, about 538.0 eV)[17]. Furthermore, these surface N/O-containing groups would enhance the hydrophilicity and wettability of the HPNOC electrode in aqueous KOH solution[11], which makes the electrolyte easily impregnate into the inner pore sur-/interfaces as large as possible for even higher surface utilization towards improved electrochemical behaviors.

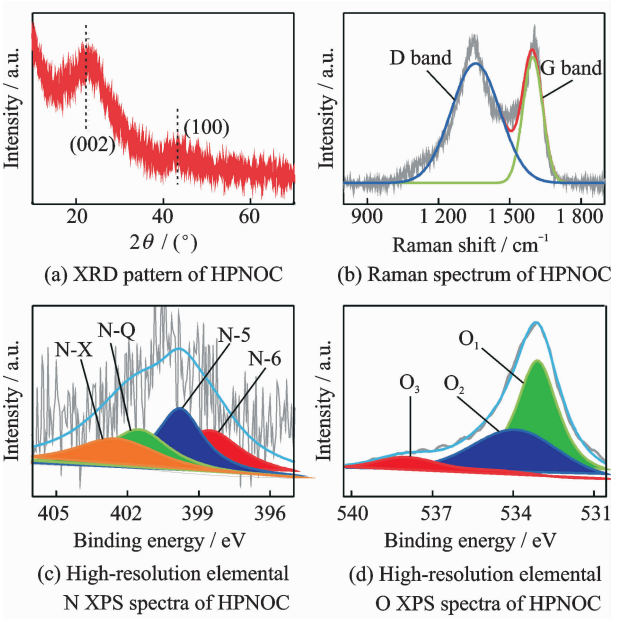

Fig. 2 XRD pattern, Ramam spectrum and XPS spectrum of HPNOC product

Table 1 Corresponding XPS of elements N and O and fitted data for the HPNOC sample

Sample		Binding energy / eV	Content (in atom)/%
N	N-6	398.5	0.50
	N-5	399.8	0.52
	N-Q	401.5	0.43
	N-X	402.5	0.45
O	O_1	533.1	6.21
	O_2	533.8	3.41
	O_3	538.0	0.58

To get more information about the pore structure of the HPNOC sample, we measured N_2 sorption isotherms accordingly. The typical adsorption-desorption isotherm of the HPNOC, as shown in Fig. 3(a), is approximately a combination of the types I and IV according to the IUPAC classification. The unique isotherm plots observed in Fig. 3(a) indicate the co-existence of rich micro-/mesopores in the sample, which can be further verified by its pore size distribution plots (Fig. 3(b)). Corresponding pore parameters of the HPNOC are collected in Table 1. The large SSA of about 2 624 $m^2 \cdot g^{-1}$, much larger than that of the sample without activation (about 65 $m^2 \cdot g^{-1}$), calculated from the adsorption

branch and high total pore volume of about 1.35 $cm^3 \cdot g^{-1}$, extremely benefits the electrolyte accessibility to the HPNOC surface for rapid charge storage. Furthermore, about 83% of the porosity is attributed by micropores (1.12 $cm^3 \cdot g^{-1}$) in the resulted HPNOC, which is beneficial for efficient charge storage[3,11]. The mseopore size distribution plot (Fig. 3(b)) derived from BJH method reveals that the mesopore size of the HNPCs is mainly located from about 3.4 nm to 3.8 nm, while there is broad micropore distribution (the inset in Fig. 3(b)) evaluated by DFT method. Accordingly, the average pore size of the HPNOC is calculated as about 2.1 nm. One should note that the hierarchical porosity of the HPNOC electrode, including micropores for electrolyte ion adsorption, and mesopores for low ion movement resistance and short ion diffusion distance[1-3], make it promising for advanced EDLCs as an electrode material.

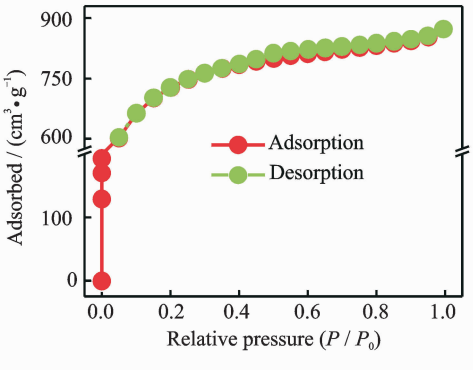

(a) N_2 sorption isotherms of HPNOC

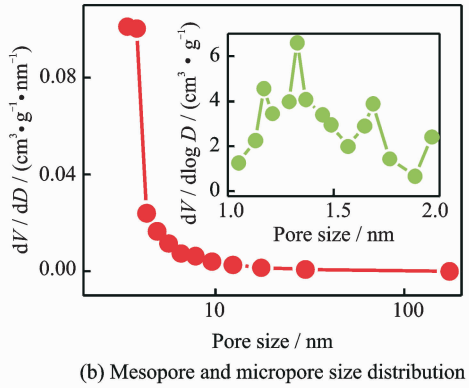

(b) Mesopore and micropore size distribution of HPNOC (The inset in panel b)

Fig. 3 N_2 sorption isotherms and size distribution of the HPNOC product

2.2 Electrochemical performance

Owing to large SSA, bi-model micro/mesopores, surface wettability and heteroatom functionalization in the HPNOC sample, the as-prepared HPNOC can be highly anticipated as a high-performance electrode with superior electrochemical behaviors for next-generation EDLCs. A series of electrochemical evaluations were thus performed in 6 mol KOH electrolyte. Fig. 4(a) comparatively plots the CV curves of the HPNOC and carbon electrode without $KHCO_3$ activation. The higher electrochemical responses in both cathodic and anodic processes are observed for the HPNOC electrode, when compared with those for the carbon electrode without activating, which indicates the higher charge-storage capability of the HPNOC. Moreover, the rectangular shape with even quicker current response on potential reversals, as evidenced in Fig. 4(a), confirms the much better electrochemical capacitances of the resulted HPNOC. Fig. 4(b) illustrates the CV curves at different scan rates from 10 $mV \cdot s^{-1}$ to 100 $mV \cdot s^{-1}$ in a three-electrode system. The observed quasi-rectangular shape in the potential window from 0.0 V to 1.0 V (vs SCE) even at a sweep rate as high as 100 $mV \cdot s^{-1}$ verifies the characteristic double-layer capacitance of the HPNOC in nature. As the scan rate increases, the curves still can keep quasi-rectangular shape and respond quickly when the voltage reverses, suggesting the high-power properties of the HPNOC in 6 Mol KOH. Fig. 4(c) shows the GCD profiles of the HPNOC with different current densities ranged from 0.5 $A \cdot g^{-1}$ to 10 $A \cdot g^{-1}$. Striking symmetry in the triangular appearance of the GCD plots testifies the outstanding electrochemical reversibility of the HPNOC during charge/discharge processes.

Corresponding gravimetric capacitances as a function of current rate are calculated with the GCD data (Fig. 4(c)), and are summarized in Fig. 4(d). Encouragingly, the HPNOC electrode obtains capacitances of about 373.6, 336.3, 315.2, 303.2, 288.4, 271.0 and 260.4 $F \cdot g^{-1}$ at current densities of 0.5, 1, 2, 3, 5, 8, 10 $A \cdot g^{-1}$, respectively. Notably, the carbon electrode without activation just delivers a capacitance of a-

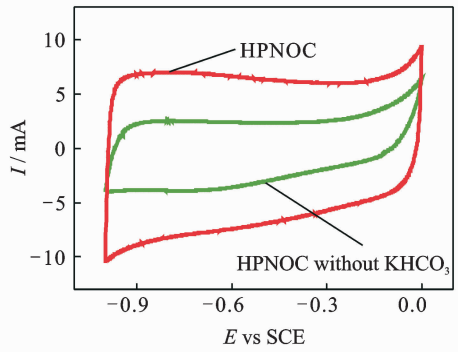

(a) CV curves at 5 mV / s of HPNOC and resultant sample without $KHCO_3$ activation

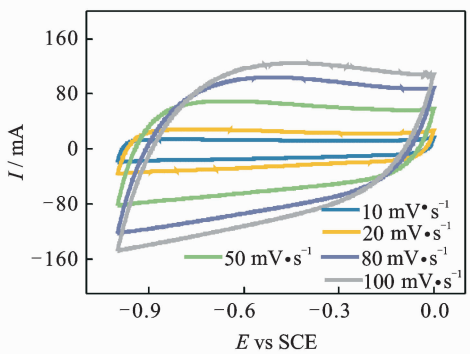

(b) CV curves of HPNOC

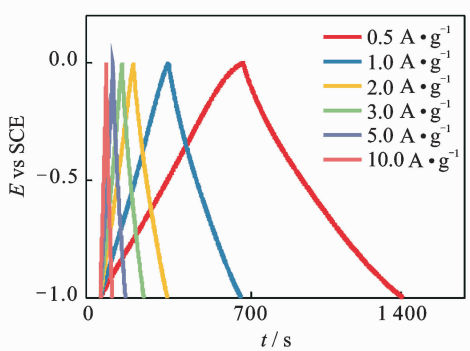

(c) GCD plots of HPNOC

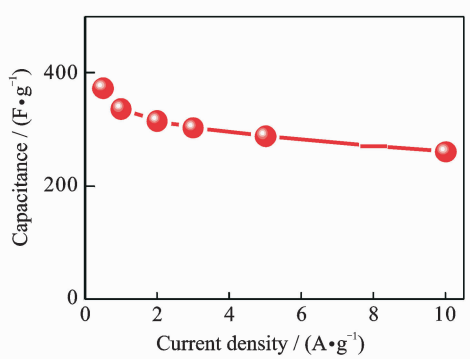

(d) Capacitance vs. current density of HPNOC

Fig. 4 Electrochemical performance in three-electrode system with 6 mol KOH electrolyte

bout 108.4 $F \cdot g^{-1}$ at 1.0 $A \cdot g^{-1}$. More remarkably, the capacitance values of our HPNOC electrode are much higher than many reported bio-mass-derived carbon materials, such as, popcorn (about 245 $F \cdot g^{-1}$ at 0.5 $A \cdot g^{-1}$)[8], stiff silkworm (about 304 $F \cdot g^{-1}$ at 1 $A \cdot g^{-1}$)[9], hexagonia apiaria (about 324 $F \cdot g^{-1}$ at 1 $A \cdot g^{-1}$)[10], rose multiflora (about 340 $F \cdot g^{-1}$ at 0.5 $A \cdot g^{-1}$)[11], cashmere (about 360 $F \cdot g^{-1}$ at 0.5 $A \cdot g^{-1}$)[12], shiitake (about 315 $F \cdot g^{-1}$ at 0.5 $A \cdot g^{-1}$)[13], lignite (about 216 $F \cdot g^{-1}$ at 0.5 $A \cdot g^{-1}$)[14], tobacco rods (about 263.6 $F \cdot g^{-1}$ at 0.5 $A \cdot g^{-1}$)[18], other porous N-doped carbon materials[3,19,20], even commercial carbon nanotubes[21], template carbon[22] and reduced graphene oxide film[23]. Additionally, as the current density increases from 0.5 $A \cdot g^{-1}$ to 10 $A \cdot g^{-1}$, the capacitance retention of about 70% strongly suggests the outstanding rate performance of the HPNOC electrode material in 6 Mol KOH aqueous electrolyte.

Furthermore, a symmetric device was assembled to investigate the practical application of the electroactive HPNOC material. Fig. 5(a) displays typical CV curves of the HPNOC-based symmetric cell with a wide scanning rate range from 5 $mV \cdot s^{-1}$ to 100 $mV \cdot s^{-1}$ in an electrochemical window with an upper potential of 1.0 V. Notably, the symmetric device exhibits quasi-rectangular shape voltammetry with respect to the zero-line and rapid current response on each voltage reversal, even at a high sweep rate of 100 $mV \cdot s^{-1}$, indicating superior electrochemical behaviors of the device with 6 mol KOH as the aqueous electrolyte.

The super symmetric GCD data (Fig. 5(b)) with linear charge-discharge plots shows the good electrochemical capacitances of the cell. More appealingly, the large capacitances can be calculated as about 69.3, 67.4, 64.8, 63.0, 60.0, 57.6, and 54.0 $F \cdot g^{-1}$ at various current rates of 0.5, 1, 2, 3, 5, 8, 10 $A \cdot g^{-1}$, respectively, as collected in Fig. 5(c), that is, a capacitance retention of about 77.9 $F \cdot g^{-1}$ can be obtained when the current density is up to 10 $A \cdot g^{-1}$. Fig. 5(d) illustrates the Ragone plot of the symmetric device. Promisingly, the device renders a high SED of about 9.6 $W \cdot h \cdot kg^{-1}$ at a power density of 0.5 $kW \cdot kg^{-1}$, and even about 7.5 $W \cdot h \cdot kg^{-1}$ at a

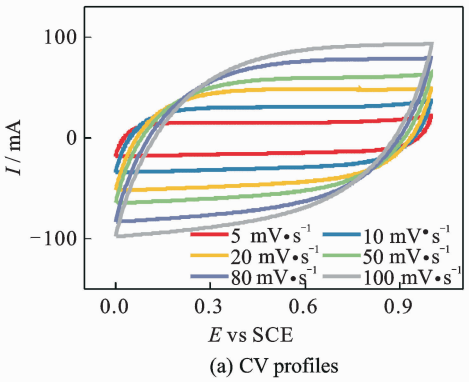

(a) CV profiles

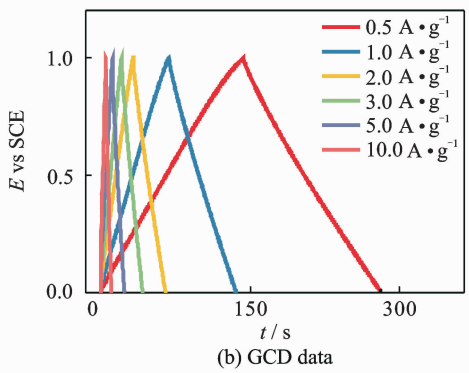

(b) GCD data

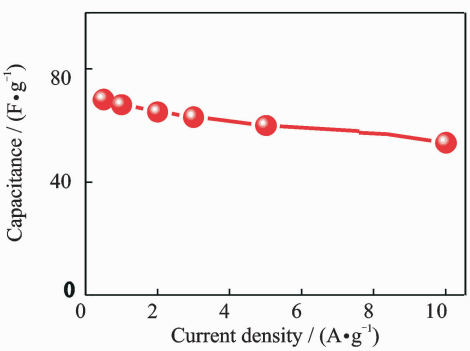

(c) Capacitance as a function of current density

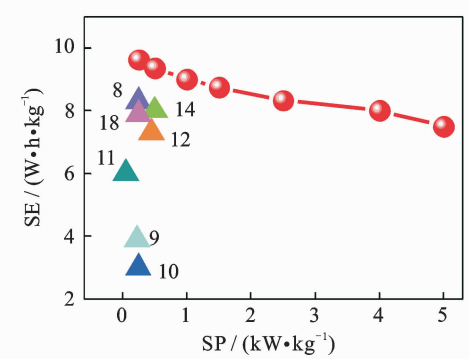

(d) Ragone plot

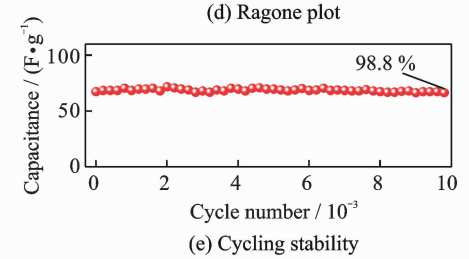

(e) Cycling stability

Fig. 5 Electrochemical performance of the HPNOC-based symmetric device

high rate of 5 $kW \cdot kg^{-1}$, which are higher than other biomass-derived carbon symmetric devices[8-12,14,18]. More encouragingly, the HPNOC-based symmetric cell shows outstanding capacitance retention of about 98.8 % after 10 000 continuous charge-discharge cycles at a large current rate of 1 $A \cdot g^{-1}$, as depicted in Fig. 5(e). The average capacitance degradation of 0.012% per 100 cycles reveals its excellent electrochemical stability of the HPNOC electrode for practical high-rate applications.

3 Conclusions

We successfully fabricated a high-performance HPNOC electrode material via mild yet green $KHCO_3$-activating strategy by using the natural blighted grains as the raw material. Of note, the synthetic method we developed here was eco-friendly, scalable, low-cost and highly repeatable for its commercial applications. The as-resulted HPNOC displayed a competitive capacitance of about 373.6 $F \cdot g^{-1}$ at a current rate of 0.5 $A \cdot g^{-1}$, high energy density of about 9.6 $W \cdot h \cdot kg^{-1}$, and superior electrochemical stability (about 98.8% capacitance retention) over 10 000 charge-discharge cycles at 1 $A \cdot g^{-1}$, which were from its unique pore structure and efficient heteroatom functionalization. More significantly, the mild activator of $KHCO_3$ is hugely promising for other biomass-based carbon materials for energy storage applications.

Acknowledgements

This work was supported by the National Natural Science Foundations of China (Nos. 51572005, 51772127).

References:

[1] WANG G P, ZHANG L, ZHANG J J. A review of electrode materials for electrochemical supercapacitors[J]. Chemical Society Reviews, 2012,41(2): 797-828.

[2] ZHANG L L, ZHAO X S. Carbon-based materials as supercapacitor electrodes[J]. Chemical Society Reviews, 2018,38(9):2520-2531.

[3] WANG Q, YAN J, FAN Z J. Carbon materials for high volumetric performance supercapacitors:Design,

progress, challenges and opportunities[J]. Energy & Environmental Science, 2016,9(3):729-762.

[4] KIM W, JOO J B, KIM N, et al. Preparation of nitrogen-doped mesoporous carbon nanopipes for the electrochemical double layer capacitor[J]. Carbon, 2009,47(5):1407-1411.

[5] WANG D W, LI F, YIN L C, et al. Nitrogen-doped carbon monolith for alkaline supercapacitors and understanding nitrogen-induced redox transitions[J]. Chemistry-A European Journal, 2012,18(17):5345-5351.

[6] ZHAO L, FAN L Z, ZHOU M Q, et al. Nitrogen-containing hydrothermal carbons with superior performance in supercapacitors[J]. Advanced Materials, 2010,22(45):5202-5206.

[7] HOU L R, LIAN L, YUAN C Z, et al. Mesoporous N-containing carbon nanosheets towards high-performance electrochemical capacitors[J]. Carbon, 2013,64:141-149.

[8] LIANG T, CHEN C L, LI X, et al. Popcorn-derived porous carbon for energy storage and CO_2 capture [J]. Langmuir, 2016,32(32):8042-8049.

[9] GONG C C, WANG X Z, MA D H, et al. Microporous carbon from a biological waste-stiff silkworm for capacitive energy storage[J]. Electrochimica Acta, 2016,220:331-339.

[10] DENG L B, ZHONG W H, WANG J B, et al. The enhancement of electrochemical capacitance of biomass-carbon by pyrolysis of extracted nanofibers[J]. Electrochimica Acta, 2017,228:398-406.

[11] CHEN Q L, SUN J F, WANG Z L, et al. Sustainable rose multiflora derived nitrogen/oxygen-enriched micro-/mesoporous carbon as a low-cost competitive electrode towards high-performance electrochemical supercapacitors[J]. RSC Advances, 2018, 8: 9181-9191.

[12] ZHOU L, CAO H, YUAN C Z, et al. Hierarchical micro-/mesoporous N- and O-enriched carbon derived from disposable cashmere: A competitive cost-effective material for high-performance electrochemical capacitors[J]. Green Chemistry, 2015,17(4): 2373-2382.

[13] CAO H, CHEN Z Y, YUAN C Z, et al. A shiitake-derived nitrogen/oxygen/phosphorus co-doped carbon framework with hierarchical tri-modal porosity for high-performance electrochemical capacitors[J]. RSC Advances, 2016,6(85):81527-81533.

[14] ZHU S Q, CHEN Q L, SHI Y Y, et al. Lignite-derived mesoporous N- and O-enriched carbon sheet: A low-cost promising electrode for high-performance electrochemical capacitors[J]. J Solid State Electrochemistry, 2016,20(3):713-723.

[15] HWANG S, LEE S, YU J S. Template-directed synthesis of highly ordered nanoporous graphitic carbon nitride through polymerization of cyanamide[J]. Applied Surface Science, 2007,253(13):5656-5659.

[16] BARRANCO V, LILLO-RODENAS M A, LINARES-SOLANO A, et al. Amorphous carbon nanofibers and their activated carbon nanofibers as supercapacitor electrodes[J]. The Journal of Physical Chemistry C, 2010,114(22):10302-10307.

[17] TIAN K, LIU W J, ZHANG S, et al. Improving capacitance by introducing nitrogen species and defects into graphene [J]. Chem Electro Chem, 2015,2(6): 859-866.

[18] ZHAO Y Q, LU M, TAO P Y, et al. Hierarchically porous and heteroatom doped carbon derived from tobacco rods for supercapacitors [J]. Journal of Power Sources, 2016,307:391-397.

[19] ZHOU Q H, CHANG J, JIANG Y T, et al. Fast charge rate supercapacitors based on nitrogen-doped aligned carbon nanosheet networks [J]. Electrochimica Acta, 2017,251:91-98.

[20] LI Y J, WANG G L, WEI T, et al. Nitrogen and sulfur co-doped porous carbon nanosheets derived from willow catkin for supercapacitors[J]. Nano Energy, 2016,19:165-175.

[21] YUAN C Z, SHEN L F, LI D K, et al. Comparative study of electrochemical capacitance of multi-walled carbon nanotubes before and after chopping[J]. Applied Surface Science, 2010,257:440-445.

[22] WEI J, ZHAO D D, SUN Z K, et al. A controllable synthesis of riche nitrogen-doped ordered mesoporous carbon for CO_2 capture and supercapacitors[J]. Advanced Functional Materials, 2013, 23(18): 2322-2328.

[23] YUAN C Z, ZHOU L, HOU L R. Facile fabrication of self-supported three-dimensional porous reduced graphene oxide film for electrochemical capacitors [J]. Materials Letters, 2014,124:253-255.

Ms. **Chen Zhiyi** received the B. S. degree from Anhui University of Technology in 2015. She joined in Anhui University of Technology in 2015, where she is a graduate student at School of Materials Science & Engineering. Her research focuses on the design and synthesis of advanced carbon materials for supercapacitors and sodium-ion batteries.

Mr. **Wang Zhengluo** received the B. S. degree from Anhui

University of Technology in 2016. He joined in Anhui University of Technology in 2016, where he is a graduate student at School of Materials Science & Engineering. His research interests mainly focus on the design and controllable-fabrication of high-performance electrode materials for lithium-ion batteries and supercapacitors.

Mr. **Zhao Zhiwei** received the B. S. degree from Anhui University of Technology in 2016. He joined in Anhui University of Technology in 2016, where he is a graduate student at School of Materials Science & Engineering. His research focuses on the synthesis and application of carbonate materials for Li-ion batteries.

Ms. **Sun Xuan** received the M. S. in 2014 and B. S. degrees in 2017 from University of Jinan, respectively. She again joined in University of Jinan in 2017, where she works as a Ph. D. candidate at School of Materials Science & Engineering. Her research focuses on the synthesis and characterization of MXene-based materials for energy storage applications (Li-ion and Na-ion batteries).

Prof. **Hou Linrui** received her M. S. degree from Xinjiang University in 2007 and Ph. D. degree from Nanjing University of Technology in 2010, respectively. She is currently a full professor at School of Materials Science and Engineering in the University of Jinan. Her current research interests are optoelectronic informational materials and relevant fields.

Prof. **Yuan Changzhou** received the M. S. degree from Xinjiang University in 2006 and Ph. D. degree from Nanjing University of Aeronautics and Astronautics in 2009, respectively. He is now a full professor at School of Materials Science and Engineering in the University of Jinan. His research focuses on the design and synthesis of micro-/nanostructured materials towards their applications in energy conversion and storage, including supercapacitors, Li/Na-ion batteries, Li-S batteries, and energy-storage photocatalysts.

(Production Editor: Zhang Huangqun)